Uniport Journal of Engineering and Scientific Research (UJESR)

Vol. 6, Issue 2, 2022, Page 110-119
ISSN: 2616-1192

(www.ujesr.org)

Analytical Evaluation of Fatigue Damage Events in Shafts

Odi-Owei, S, Nkoi, B and Ayoka, K.E
Department of Mechanical Engineering, Faculty of Engineering
Rivers State University, Port Harcourt Nigeria
*Corresponding author's email: steveodiowei252@gmail.com

Abstract
This study analyzed a rotating machine component, AISI 1020 steel and carbon-fibre composite shaft of circular cross section, under fatigue loading. Finite element shaft models were generated to show increased deformation. The crack (1 mm in length) was created via classical analytical approach and shown to restrict the load capacity of the shaft. The shaft model of typical composite materials was subjected to reversed stresses of specified magnitudes. The Finite Element Analysis (FEA) tool using Matlab code was utilized to evaluate the state of strength and stiffness. Another computational tool used was the Mathematical (Classical Analytical) Methods in Engineering. Mathematical models have appropriate parameter values for mechanical analysis and design of parts for fatigue loading. Partial differential equations were computationally more efficient for solving specific boundary-value problems and components of the new stress state of the shaft. Satisfying the defined crack boundary conditions indicated that the shaft can operate at an acceptable degree of safety after accumulating a prescribed level of damage (crack size). A minimum fibre diameter of two micrometers gave a maximum fibre strength of 4.5 GPa. The resulting redistribution of stress components was expressed using Westergaard's method. Crack-tip component stresses were expressed in terms of the properties of the composite material shaft. It was shown that changes in stiffnesses and strengths were dependent on lamina orientation angles and fibre diameters. It was also found that damage produced cracks with stress singularity at the crack-tip.
Keywords: *Fatigue strength, Fatigue damage, Crack opening, Crack-tip stresses, Stiffness*

Received: 13th April, 2022 *Accepted: 29th June, 2022*

1. Introduction

The fatigue problem consists of analyzing the strength of a given piece of shaft when subjected to cycles of deterministic or random loads. This can influence future design decisions on material characterization, load configuration in automobile drive shaft, and airplane rotor blades. Degradation of parts under cyclic stresses occurs by a combination of damage modes and mechanisms. Pre-existing loading condition and associated deformation influence the generally accepted state of the material, especially the state of stress. It is well known that the static strength of a piece, that is, the static stress resisted by the piece without failure, is much higher than the stress resisted if this stress is repeated many times. This repetition of small stresses frequently causes crack opening Mode I, found by using parallel mathematical developments, and Mode II determined by forward shear (Reifsnider, 1990). In addition to that, due to small repeated stresses failure of many real-world structures occur unexpectedly. The phenomenon is complicated and only partially understood. In this work, computed primary parameters will aid others, reductions in stiffness and strengths analyzed using the Finite Element Method, and satisfied boundary conditions determine varying end-point stresses.

Physical details of damage define the fatigue effect. These control the state of stress, the state of strength (an inherent property of the part), and stiffness changes (controlled by the state of stress). The fatigue problem, in this work, is also defined by subjecting the shaft to torsion and bending stresses varying with rotation. With the state of weakness, strength is reduced as well as the stiffness, indicating evidences of damage. Fatigue strength during cyclic loading is of crucial importance in real life. Fatigue is characterized by cracks that initiate at discontinuities as a result of repeated or cyclic stresses. The crack is dynamic Freund (1990) and the role of stress waves is

distinct. Crack initiation is clear evidence of damage due to the fatigue phenomenon. In Mode I crack loading, external forces open up crack faces. This results in stress redistribution at the crack-tip. Tensile waves propagate across the body and reload the crack-tip.

The problem is very challenging. Cracks subjected to nominal Mode I loading actually open in mixed Modes I and II. Crack loading Mode II is in-plane shear with stress components as in the case of mode I (Lankford and Davidson, 1983). Factors influencing the crack growth include minimum/maximum stress ratio (Chen, 2013), microstructure, surface discontinuities, etc. Partial differential equations are computationally more efficient (Airy, 1863) for solving specific boundary-value problems and components of the new stress state of the shaft. Field equations are derived (Reifsnider, 1991) to describe the motion of the crack tip in two-space dimensions. The 2D stress element has four stress components determined on the basis of symmetry. This will involve the generation of parameters for the mathematical model. It is hoped that this study yields expressions for crack-tip stress components on the shaft.

The stress field ahead of the crack is dominated by the stress intensity factor, K. Westergaard's solution was simplified (Irwin, 1957) in the area immediately surrounding the crack tip. There are coefficients in crack-tip stress expansions for two collinear finite cracks of equal length in an infinite plane medium. Based on the solutions of complex variable theory in plane elasticity, the stress field near the crack tip at infinity can be obtained (Stepanova and Roslyakov, 2016). An efficient simulation method for fatigue behaviour of structures successfully expand to consider not only damage but also plastic deformation accumulations due to fatigue (Junsong et al., 2017). Crack formation and growth can be analyzed by means of fracture mechanics and finite elements. Based on the simulation method, the damage distribution and the potential fatigue damage failure pattern could be reasonably predicted by finite element analysis (Hasegawa and Smadel, 2018). There are established rules of reference fatigue crack growth rates and the fatigue crack growth thresholds for ferritic steels. They were provided by many fitness-for-service (FFS) codes. The thresholds provided by the FFS codes can be introduced and the threshold was analyzed by using crack closure.

A novel comprehensive modelling approach used to simulate the complex fretting wear process provides information to assess the critical instant for crack initiation (Zeise et al., 2014) during the redistribution of stresses. The current state of the material and the state of stress (Reifsnider and Talug, 2018) are dependent upon the history of prior loading and associated deformation. Factors influencing the crack growth include minimum/maximum stress ratio (Chen, 2013) microstructure, surface discontinuities, etc. With the state of weakness, strength is reduced as well as the stiffness, indicating evidences of damage. Non-destructive vibration test data is used to detect structural damage. The analysis can be based on the assumption that damage will change the structural (mass, stiffness or damping) properties which (He, 2009) leads to changes in the dynamic characteristics such as the natural frequencies, damping loss factors and mode shapes. Sanford (2013) stated that crack growth data can be presented in the form of the crack propagation behaviour described in the most general terms. He introduced the K factor to make the result conform to current notation. The result is the Cartesian stress components in the neighbourhood of a crack-tip. In this paper, finite element models were developed for fatigue damage events in shafts. The Solid works software and MATLAB code were utilized to evaluate the state of strength and stiffness. Classical Analytical approach was also used to carry out the crack-tip stress analysis.

2. Materials and methods

2.1 Fatigue damage accumulations in the shaft

Damage is the event and process that combine in a way that alters the state of the shaft, and change the response to the extent that it may fail to satisfy its intended service requirements. The focus is on the mechanics of damage development in the shaft. It is uncommon for a single crack to dominate the damage development and fracture process. So, the damage mechanism of matrix cracking is involved. Interface de-bonding results in interface shear stress. In interface wear, solid particles are loosened from the surface. The damage evolution dissipates energy. The shaft in this work (Fig. 1) is loaded by a standard non-rotating force of 7.0 kN.

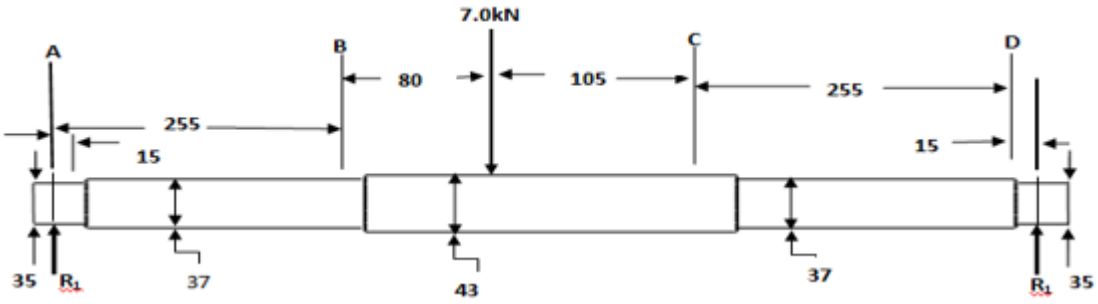

Fig. 1: Shaft model (all dimensions in mm and fillets, 3 mm radius)

The physical theory and internal working of the computer to generate the FEA values obtained are explained with the relation between displacements and strains. For the steel, normal strain, ϵ_x, in the x-direction is the ratio of change in length to original length,

$$\text{i.e. } \epsilon_x = \frac{L_2 - L_1}{L_1} = \frac{\left[dx+\left(u+\frac{\partial u}{\partial x}dx\right)-u\right]-dx}{dx} = \frac{\partial u}{\partial x} \qquad (1)$$

A similar analysis gives the normal strain in the y-direction, $\epsilon_y = \frac{\partial v}{\partial y}$ (2)

where L_2 = new length, L_1 = original length, u,v = displacements and functions of xy, $\frac{\partial u}{\partial x}dx$ = displacement increments.

Shear strain γ_{xy}=change in right angle = $\frac{\left[u+\left(\frac{\partial u}{\partial y}dy\right)-u\right]}{dy}+\frac{\left[v+\left(\frac{\partial v}{\partial y}dx\right)-v\right]}{dx}=\frac{\partial u}{\partial y}+\frac{\partial v}{\partial x}$ (3)

In two-dimensional matrix operator form

$$\begin{Bmatrix}\epsilon_x\\ \epsilon_y\\ \gamma_{xy}\end{Bmatrix}=\begin{bmatrix}\frac{\partial}{\partial x} & 0\\ 0 & \frac{\partial}{\partial y}\\ \frac{\partial}{\partial y} & \frac{\partial}{\partial x}\end{bmatrix}\begin{Bmatrix}u\\ v\end{Bmatrix} \qquad (4)$$

If stresses are arrayed in the order,

$$\{\sigma\} = \lfloor\sigma_x \quad \sigma_y \quad \tau_{xy}\rfloor^T \qquad (5)$$

Then the equilibrium equation is

$$[\partial]^T\{\sigma\}+\{F\}= \{0\} \qquad (6)$$

where $\{F\}$ is $\lfloor F_x \quad F_y\rfloor^T$ and $\{\sigma\}$ is $\frac{\lfloor F_x \quad F_y\rfloor^T}{[\partial]^T}$

For the composite materials, the strains are linear functions of the distance z from the still unknown neutral axis. The normal stress σ_{zz} is zero. This material is subjected to conditions of plane stress. To derive the stress-strain relations for plane stress in orthotropic materials, it can be considered that a thin layer of material lies in the xy plane, and recall that all stresses in the z direction are zero. This can be put in matrix form; three equations that give normal stresses in terms of normal strains and three that give shear stresses in terms of shear strains. Then the normal strains in terms of normal stresses and shear strains in terms of shear stresses are determined. A tensile strength applied to the:

x faces of the element is $\sigma_{xx} = E_x\varepsilon_{xx}$ (9)

y faces of the element is $\sigma_{yy} = E_y\varepsilon_{yy}$ (10)

z faces of the element is $\sigma_{zz} = E_z\varepsilon_{zz}$ (11)

where E_x, E_y and E_z are Young's moduli in the x, y, and z directions, respectively. Because the material is orthotropic, these quantities which are called generalized Young's moduli are not equal. Extension of the element in the x-direction is accompanied by a contraction in the y and the z-directions. So,

$$\varepsilon_{yy} = -\nu_{xy}\varepsilon_{xx}, \qquad \varepsilon_{zz} = -\nu_{xy}\varepsilon_{xx}, \qquad (12)$$

where ν_{xy} and ν_{xz} are Poisson ratios, the subscript x is the direction of a unit strain, and y and z are the directions of the contraction of ν_{xy} and ν_{xz} respectively. In compact form

$\{\boldsymbol{\varepsilon}\} = [\,\bar{\boldsymbol{S}}\,]\,\{\boldsymbol{\sigma}\}$ where $\{\boldsymbol{\sigma}\}$ is $[\sigma_{xx} \;\; \sigma_{yy} \;\; \sigma_{xy}\,]^{\boldsymbol{T}}$, $\{\boldsymbol{\varepsilon}\}$ **is** $[\varepsilon_{xx} \;\; \varepsilon_{yy} \;\; \gamma_{xy}\,]^{\boldsymbol{T}}$ and

$$\text{the stiffness } [\bar{S}] = -\begin{pmatrix} \frac{1}{E_x} & -\frac{v_{yx}}{E_y} & 0 \\ \frac{v_{yx}}{E_y} & \frac{1}{E_y} & 0 \\ 0 & 0 & \frac{1}{G_{xy}} \end{pmatrix}$$

In this work, the description of damage in steel and composite shafts under fatigue is based on actual mechanical events which form the mechanisms of damage development. After thousands of cycles of loading, cracks initiate as one of the results of damage due to fatigue. The shaft design is based on the stress at which the failure theory predicts that the weakest portion will fail. The physical situation corresponding to the weakest portion of failure is imagined to be cracking. The fundamental nature of fatigue as a physical process has fundamental aspects of mechanics representations of the process. It is believed that all fatigue damage processes are non-conservative. From the standpoint of mechanics, this means that the current state of the material and state of stress are dependent upon the history of prior loading and associated deformation.

2.2 Degradation of stiffness due to damage

Prediction of stiffness loss in this study is by using the deformations and shaft orientation angles. The shaft is rotated many times, and the procedure used to process input force and quantify deflection. Stiffness reductions from damage growth are load-history dependent. The damage that reduced stiffness was due to increase in deflection around the section of the shaft undergoing reversed stresses. This can be shown as the stiffness K is the ratio of applied force F to the deformation (elongation) e. The rigidity is lowered as elongation increased and stiffness then goes down. As the deflection increased from its level during the first few cycles of loading, the natural frequency also lessened, indicating loss in stiffness. Steel stiffness, as the applied force per unit deflection, was high initially so that any effect from torsional vibration is negligible. However, the stiffness decreased as deflection increased.

2.3 Strength reduction in fatigue loaded shafts

To discuss properly the mechanics of strength during cyclic loading, it is necessary to determine the state of stress and the state of the material in a continuous fashion. As cycles increased, elastic tensile loading and unloading followed by compressive reloading, showed reduction in strength. In addition to this, using the procedure of front-and-back shaft bending, the force required to produce the same deflection got lower and lower as the cross-sectional area remained constant and cycles increased. This is an indication of lower and lower strength. The shaft's elastic tensile loading to positive maximum strength is unloaded and reloaded in compression to negative maximum strength. Each cycle of loading is characterized by yielding and cracking. Failure by cracking results from the reversing bending stresses. When the strength reductions reach the applied stress level, fracture occurs.

2.4 Cracks as physical evidence of damage in shaft fatigue loading

After thousands of cycles of loading, cracks initiated as one of the results of damage due to fatigue. There are some differences in the crack opening stresses, having as principal cause the different plasticity that the models suffered, due to propagation rates.

2.4.1 Mode I crack opening elastic fields

In this work, as the damage process alters the local geometry as a function of the number of applied cycles of loading, the internal stress redistributes continuously in time, and gives rise to further damage development. Fatigue cracks loaded in scanning electron microscope show crack in ModeI loading. In Figure 2, external forces open up crack face resulting in an opening displacement and motion of the crack face.

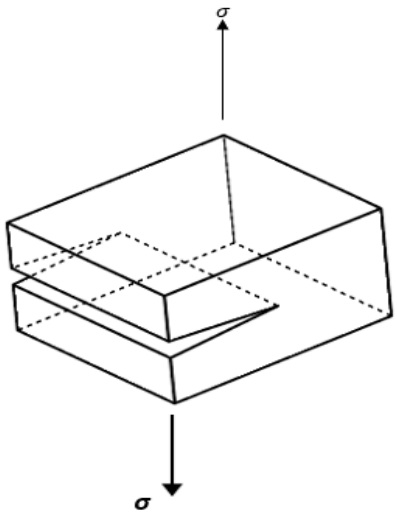

Fig. 2: Crack opening mode I

Ultimately, this localization process creates a sufficiently intense local region of damage and stress which nucleates fracture of the shaft. The cracks restrict the load capacity of the shaft. In Fig. 3, y = 0 so, the crack plane is into the paper and along the horizontal x-axis. The component stresses are functions of the second derivatives of the stress function.

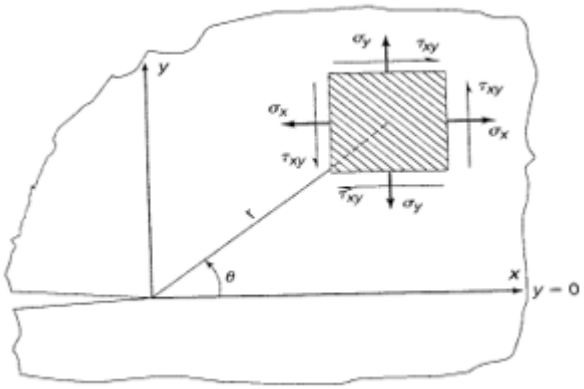

Fig. 3: The coordinates of elastic stress redistribution near crack-tip

With the crack in place, stresses are redistributed. The expressions for the components of the redistributed stress after damage are derived. After thousands of cycles of loading, cracks initiated as one of the results of damage due to fatigue. Analysis of stresses near the crack-tip led to the expressions for the stress components. To analyse the redistributed crack-tip stresses, the choice for Airy's stress function in this work is

$$\chi \equiv \text{Re}\,\bar{\bar{x}} + x_2\,\text{Im}\,\bar{x} \quad (12)$$

where x_2 is the imaginary part of the complex number, z.

with $\chi(z) = \frac{\sigma_{x_1}}{\sqrt{(1-\frac{a^2}{z^2})}}$

The stress function, χ, is related to the 2-D redistributed stress components given by

$$\sigma_{11} = \frac{\partial^2 \chi}{\partial x_2^2} \quad (13a)$$

$$\sigma_{22} = \frac{\partial^2 \chi}{\partial x_1^2} \quad (13b)$$

$$\sigma_{12} = \frac{-\partial^2 \chi}{\partial x_1 \partial x_2} \quad (13c)$$

Equation (1) is differentiated to obtain the components of the redistributed stresses after the cracking. The stresses are functions of 2nd derivatives of χ. The first derivative of Equation (1) is (using the product rule of differentiation):

$$\frac{\partial \chi}{\partial x_2} = \frac{\partial (Re\,\bar{\bar{x}})}{\partial x_2} + x_2 \frac{\partial (Im\,\bar{x})}{\partial x_2} + \text{Im}\bar{x} \quad (14)$$

Applying the rules $\frac{\partial Re\,(\bar{x})}{\partial x_1} = \frac{\partial\, Im\,(\bar{x})}{\partial\, x_2}$ changes Equation (3) to:

$$\frac{\partial\, Re\,(\bar{x})}{\partial x_2} = \frac{-\,\partial\, Im\,(\bar{x})}{\partial\, x_1} \quad (15)$$

Applying Equation (15), Equation (14) becomes:

$$\frac{\partial x}{\partial x_2} = \frac{-\,\partial (Im\,\bar{\bar{x}})}{\partial x_1} + x_2 \frac{\partial (Re\,\bar{x})}{\partial x_1} + \text{Im}\bar{x} \quad (16)$$

To solve for the expressions for the stress components, function of function rule applies,

$$\frac{\partial\,(\chi)}{\partial x_1} = \frac{\partial\,(\chi)}{\partial z}\frac{\partial z}{\partial x_1} = \frac{\partial\,(\chi)}{\partial z} \quad (17)$$

Applying Equation (17), the expression relative to z is given by:

$$\frac{\partial \chi}{\partial x_2} = \frac{-\,\partial (Im\,\bar{\bar{x}})}{\partial z} + x_2 \frac{\partial (Re\,\bar{x})}{\partial z} + \text{Im}\bar{x} \quad (18)$$

From the definition of stress function

$$\frac{\partial x}{\partial x_2} = -\,\text{Im}\bar{x} + x_2 \text{Re}\, x + \text{Im}\bar{x} \quad (19)$$

$$\Rightarrow \frac{\partial \chi}{\partial x_2} = x_2 \text{Re}\chi \quad (20)$$

The 2-D stress element has four stress elements σ_{11}, σ_{22}, σ_{21}, and σ_{12} displayed in a 2x2 diagonal symmetric matrix as shown in Equation (21). Due to the symmetry only σ_{11}, σ_{22}, and σ_{12} are obtained and$\sigma_{21} = \sigma_{12}$. These are on the crack (complex) plane. The matrix of components of the redistributed stress is given by:

$$\begin{bmatrix} \sigma_{11} & \sigma_{21} \\ \sigma_{12} & \sigma_{22} \end{bmatrix} \quad (21)$$

where σ_{11} is the x_1-component of the crack-tip stress in the x_1-direction, σ_{21} is the ix_2-component of crack-tip stresses in the x_1-direction, σ_{12} is the x_1-component of the crack-tip stresses in the x_2-direction, and σ_{22} is the ix_2-component of the crack-tip stresses in the ix_2-direction. As shown in Fig. 3 earlier, y-axis is zero. So, the crack-plane (complex plane) is along the x-axis and into the paper. Following Westergaard's method, the infinitesimal chunk of stress element (Fig. 3) taken from the shaft is linear, making it a plane (2D). The array of stress components in 2D are displayed in the 2x2 (if 3D then 3x3) matrix. The derivative of Equation (22) is now the second derivative of the stress function relative to x_2. This would be σ_{11}, representing the x_1 component of the stress in the x_1 direction. Hence,

$$\sigma_{11} = \frac{\partial^2 \chi}{\partial x_2^2} = \frac{\partial [\,x_2\ Re\,\chi]}{\partial x_2} \quad (22)$$

Applying product rule in Equation (21), the expression for σ_{11} *becomes*:

$$= x_2 \frac{\partial (Re\,\chi)}{\partial x_2} + \text{Re}\,\chi \quad (23)$$

Applying Equation (15) again, Equation (23) becomes:

σ_{11}= - $x_2\frac{\partial\, Im\, x}{\partial x_1}$+ Re χ (24)

Relative to z, see also Equation (17), the above equation can be written as:

= -$x_2\frac{\partial\, Im\, x}{\partial z}$ + Re χ (25)

Applying Equation (15) and differentiating again, we have

= - x_2 Im $\acute{x}$+ Re χ (26)

⇒ σ_{11}= -x_2 Im $\acute{x}$+Re χ (27)

where $Im\,\acute{x}$ is the imaginary part of the derivative of χ, Re χ is the real part of χ, The model derivations started with Equation (1), the stress function, and related 2D stress components Equations (13a-13c), followed by a series of applied rules. Similarly, derivative relative to x_1x_2 gives $\sigma_{12,}$ the x_1 component of the stress function in the ix_2 direction.

$\sigma_{12} = -x_2 \mathrm{Re}(x')$ (28)

σ_{12} stress component implies some shear (or overlap of axes 1 and 2). Following the same procedure, the second derivative of the stress function relative to x_1 gives σ_{22}, the ix_2 component of the stress in the ix_2 direction.

$\sigma_{22} = \mathrm{Re}(x) + x_2 \mathrm{Im}(x')$ (29)

2.4.2 Crack face boundary conditions

Stress on the crack face is zero, and at the crack-tip it is at infinity Westergaard (1939). The stress function solved is a double integral function, Equation (1). The Solution, Equation (16), was by differentiating (not by integrating to obtain the constant of integration). The crack boundary starts from zero, the point where the crack initiated (taken as the origin) to the crack length 1 mm on the real axis of the crack plane. So, the conditions are:

(1) $\sigma_{11} \rightarrow \sigma_\infty$ as $z \rightarrow x_L$ $\sigma_{22} \rightarrow \sigma_\infty$ as $z \rightarrow ix_2$ i.e. the component stress, σ_{11} tends infinity as the complex number z tends to its real part x. Stress component σ_{22} tending to infinity if z tends to its imaginary part ix, implies that it is zero as ix is negligible in that direction. In the same reasoning, σ_{12} is also zero.

(2) ($0 < x_1 < a$, $ix_2 = 0$), $\sigma_{22} = 0$ $\sigma_{12} = 0$. This means that x1 ranges from 0 to a = 1, the crack length. (1) and (2) are the boundary conditions.

Since x is the real part of z and ix (= 0) is the imaginary part, we have Equation (27) with

χ (x) = Re $[\frac{\sigma_{x_1}}{\sqrt{(1-\frac{a^2}{x^2})}}]$, a function of x instead of z as earlier. (30)

Equation (30) correlates to Westergaard's formula,

Z = Re$[\frac{\sigma_\infty}{\sqrt{(1-\frac{a^2}{z^2})}}]$ = σ_∞ (for z = 0) (31)

where Z is his choice of Airy's stress function, and σ_∞ is stress at infinity. Substituting the limits 0 and 1in Equation (32)

when x = 0, χ (x) = Re$[\frac{\sigma_{x_1}}{\sqrt{(1-\frac{a^2}{0^2})}}]$ = σ_{x_1}= 0 (32)

Infinity in the denominator, dividing a number in the numerator, gives 0 for Equation (32).

when x = 1, χ (x) = Re$[\frac{\sigma_{x_1}}{\sqrt{(1-\frac{a^2}{1^2})}}]$ = σ_{x_1}= σ_∞ (33)

Equations (32) and (33) satisfy the crack face boundary conditions; x = 0, σ_{x_1}= 0; and x = 1, σ_{x_1}= σ_∞

$\sigma = \frac{K}{\sqrt{2\pi d}}$ (Stanford, 2013) using elastic stress intensity factor, K = 200 MPa $m^{1/2}$ (34) was used to determine the end-point stresses at corresponding distances away from the crack-tip as plotted and presented in the results, Figure 9. This correlates with Westergaard's results Figure 10. The figures show that stress is at infinity at the crack-tip and 0 at the crack face. The stress values then decreased as distances from crack tip increased.

3. Results and discussion

Physical details of damage define fatigue effects. The state of stress of a shaft under fatigue loading changes from the condition at the beginning of the loading to its condition just before the on-set of cracks. The state of stress is controlled by damage to the subcritical sections and this contributes to the stress redistribution which introduces changes in the internal geometry of the shaft. Using Westergaard's 2D approach which also follows Airy's stress function rules and compatibility rules, the expressions for the components of the redistributed stress are derived. Degradation of Stiffness and Strength Reductions were determined via Finite Element Analysis (FEA) and Solved Using Matlab Code. It predicted how the shaft reacted to boundary conditions such as stresses to understand if it will work safely or not.

3.1 Accumulation of damage

From the standpoint of the direction of load application and the material orientation angle, Figure 4 was obtained through the FEA analysis (Matlab Code) for steel shaft. Load application in the transverse direction (perpendicular to the axis of the shaft) combined with increased deflection and so, large orientation angle.

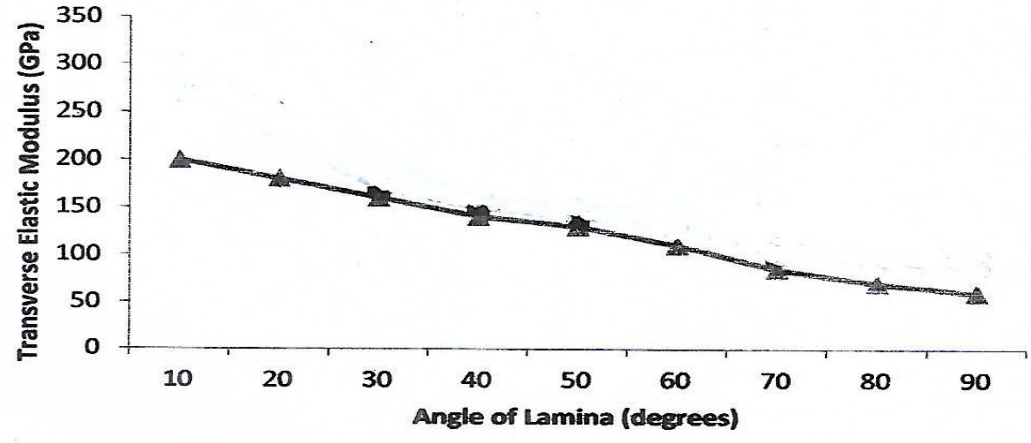

Fig. 4: Transverse elastic modulus of the steel as functions of angle of lamina

3.2 Stiffness reduction

Stiffness loss from damage growth in the shaft was load-history dependent and seen from the standpoint of deformation. The knowledge of deformations is specified in terms of strains, that is, the relative change in the size and shape of the body. Figure 5 shows the relationship between lamina angle and transverse elastic modulus. The elasticity decreases as lamina angle increases, for the composite as well. However, being composite improves the stiffness situation. Increase in deflection indicated loss in stiffness. The significance of this was that the shaft should be designed within the proportional limit to maintain rigidity.

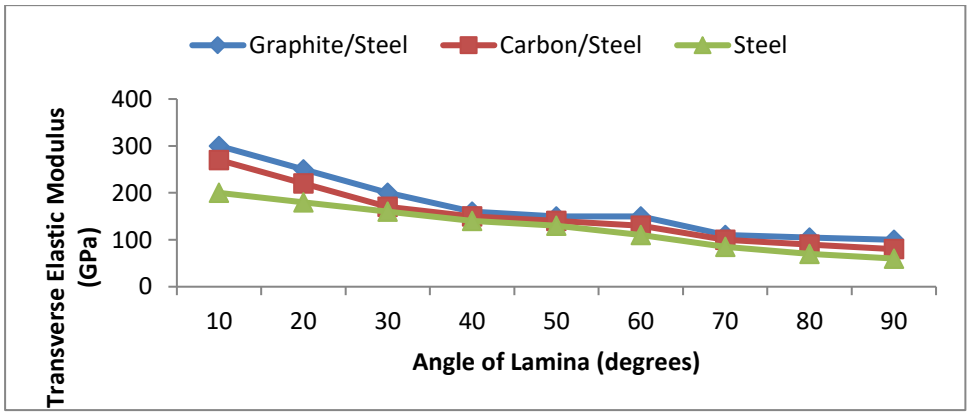

Fig. 5: Transverse elastic modulus of the composites, and steel, as functions of angle of lamina for the composites

3.3 Strength reduction

As cycles increased, elastic tensile loading and unloading followed by compressive reloading showed reduction in strength. Using the procedure of back-and-forth shaft bending, each cycle of loading is characterized by yielding and cracking. Failure by cracking results from the reversing bending stresses. In Fig. 6, fibre strengths are plotted against fibre diameters. The larger the diameter of the fibre used as laminate with the composite shaft, the smaller the strength. This was due to the inherent flaws in the material. Removal of the flaws reduced the diameter and strength would then increase. Stress, as the intensity of the load per unit area, means that the strength of a material is intrinsically known in terms of stress. The strength is based on proportional limit. The elastic tensile loading and unloading followed by compressive reloading showed reduction in strength.

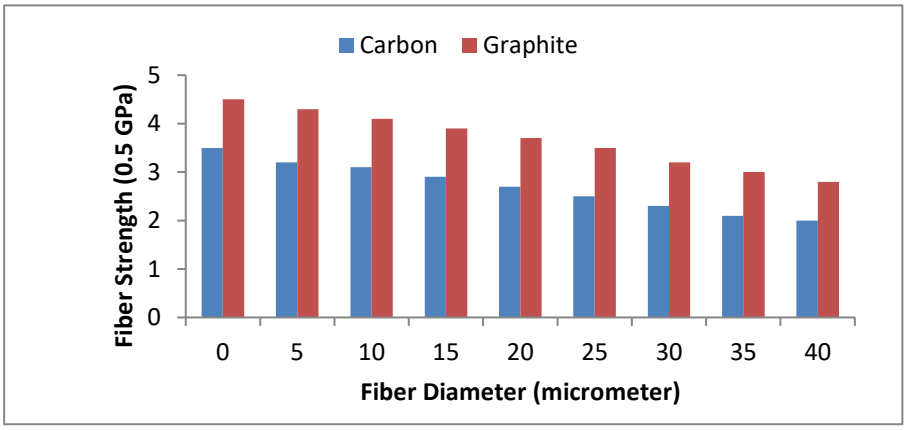

Fig. 6: Fibre strength versus fibre diameter

3.4 Cyclic-load-induced redistribution of stress

After thousands of cycles of loading, cracks initiate as one of the results of damage due to fatigue. Stress components near the crack tip were found by use of complex variable concept. Using this concept and the Cartesian co-ordinates in analyzing the crack tip stresses, components reduced to three: σ_{11}, σ_{12}, and σ_{22}. Following Westergaad's approach, expressions for the redistributed stress components were determined in forms of the complex variables.

The resulting redistribution of stress components as solved using Westergaard's method are: For Mode I loading, Equation (27), Section 2.4.1. This expression helped to keep hold of the fact that there are two aspects of this stress component, the real and imaginary. Similarly, Equations (28) and (29) resulted from Section 4.2.1 as well. In these, σ_{12} stress component implies some shear (or overlap of axes 1 and 2). In considering boundary conditions, this is shown to be zero as there is no shearing in Mode I crack opening. Also, σ_{22} component is in the ix_2-axis and in ix_2-direction all in the crack plane. Since the y-axis is zero (Fig. 3), the crack plane is in the x-axis. The crack grows in this plane as a surface phenomenon. Therefore, physically σ_{22} is imaginary. In Fig. 7, the plot of component stresses (e.g. σ_{x_1}) against distances away from the crack-tip is shown. The stresses are highest at the crack-tip and dropped (until the applied stress level) as distances from the crack-tip increased.

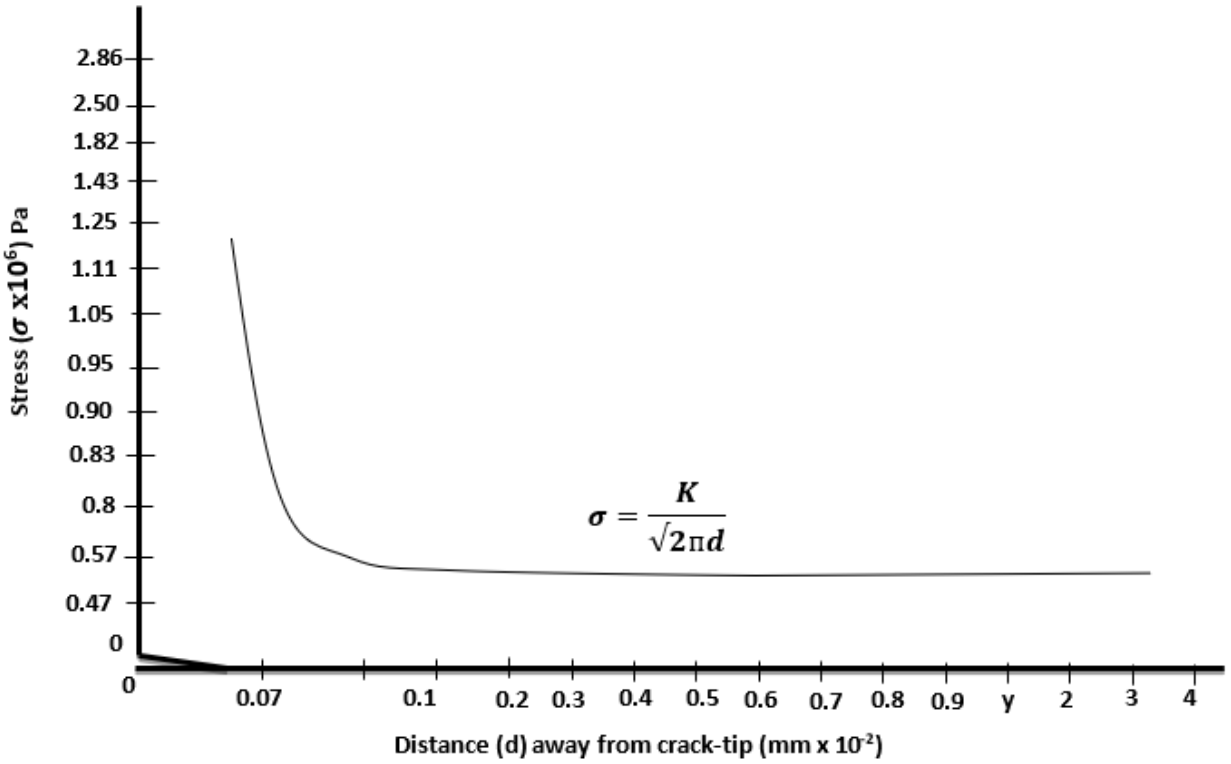

Fig. 7: Stress components against distances away from crack-tip

$\sigma = \frac{K}{\sqrt{2\pi d}}$ is a fracture mechanics concept used in design (Sanford, 2013). It is used here to determine end-point stresses. The result correlates with those of Westergaard in Fig. 8. The entire stress field is proportional to σ_{x_1}(as reflected by the equation). The graph is compared with the relationship between stress and the distance along crack plane as obtained by Westergaard. Westergaard's plot (Fig. 8) showed that stresses decreased from infinity at the crack-tip (x = a), to the far-field value of σ_∞. The closeness of results from this study to those of Irwin who simplified Westergaard's solution in the area immediately surrounding the crack-tip, further validates this work. The difference was when stress decreases to zero at a limiting point around the crack-tip signalling stress intensity. In this work, the stress function satisfied equilibrium equation and proved to be the solution for a crack in a shaft. This is seen by taking the derivatives of the stress function to get expressions for the redistributed stress components.

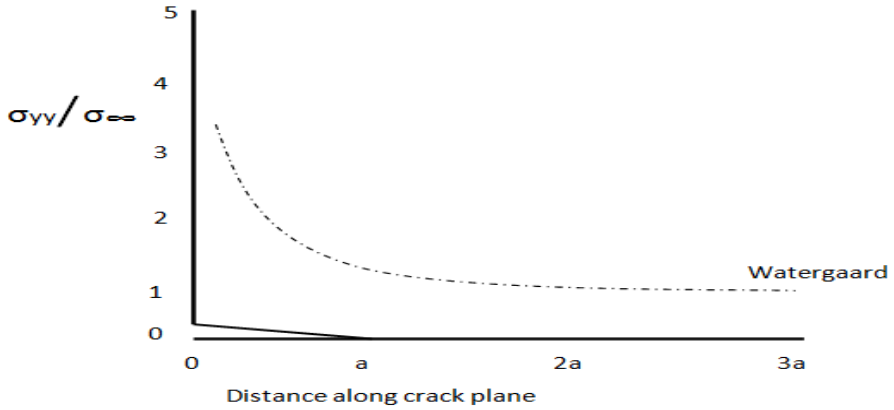

Fig. 8: Westergaard's plot of σ_{yy} and σ_∞ stress components against crack length

4. Conclusion

From the study, the following conclusions can be drawn:

i. Cyclic loading significantly reduced strength, degraded the stiffness and increased the deflection.
ii. Local stresses are altered by the formation of cracks controlled by cyclic stress level. Energy is not conserved but dissipated in driving the crack (propagation). Cracks form due to interface de-bonding enriched by internal stresses forming intense damage region.

References

Airy, G. (1863) Airy's Stress Functions: Partial Differential Equations for Boundary-Value Problem. New York, McGraw-Hill.

Chen, B. (2013) Fatigue Study of Pipeline Steels (Master's thesis). Department of Mechanical Engineering, University of Tennessee, Knoxville.

Freund, L. (1990) Dynamic Fracture Mechanics. New York: Cambridge University.

Hasegawa, K., and Stmadel, B. (2018) Definition of Fatigue Crack Growth Thresholds for Ferritic Steels in Fitness-for-Service Codes. American Society of Mechanical Engineers: Pressure Vessels and Piping Conference, 1A (1): 18-40.

Irwin, G. (1957) Analysis of Stresses and Strains Near the End of a Crack Travelling a Plate. Journal of Applied Mechanics, 24: 361-364.

Junsong, L., Xin, N., Mahadi, M., Jie, L. and Mo, Y. (2017) A Study on the Simulation Method for Fatigue Damage Behaviour of Reinforced Concrete Structures. International Journal Fracture Mechanics, 110(4): 351–369.

Lankford, J. and Davidson, D. (1983) Wear Debries due to Mode II Opening of Mode I Fatigue Cracks in an Aluminum Alloy. Metallurgical Transactions, 14A, p.1227.

Reifsnider, K.L. (1990) Fatigue of Composite Materials Edited by K.L. Reifsnider Elsevier Science Publishers B.V.

Reifsnider, K.L. (1991) Damage and Damage Mechanics. Composite Materials Series, Stores, Connecticut, 8(5): 54-60.

Reifsnider, K. and Talug, A. (2018) Analysis of Fatigue Damage in Composite Laminates. A Talug – International Journal of Fatigue, 2(1): 88-102.

Sanford, R. (2013). Principles of Fracture Mechanics. Upper Saddle River: Prentice Hall.

Stepanova, L. and Roslyakov, P. (2016) Complete Williams Asymptotic Expansion Near the Crack Tips of Collinear Cracks of Equal Lengths in an Infinite Plane Medium. Science Direct Procedia Structural Integrity 2(21): 178-196.

Westergaard, H. **(**1939) Solution for Cracks. Science Direct Procedia Structural Integrity, 2(16): 189-196.

Zeise, B., Liebich, R. and Pr*ö*IB, M. (2014) Simulation of Fretting Wear Evolution for Fatigue Endurance Limit Estimation of Assemblies. Pasedina, California: Elsevier, 40(5): 98-112.

Nomenclature

χ, choice of Airy's stress function
z, choice of a function of complex numbers
$\bar{x}$, 1st integral of χ
$\bar{\bar{x}}$, 2nd integral of χ
a, crack length
σ, stress
σ_x, x-component of σ
σ_y, y-component of σ
x_1, ix_2, complex coordinates
σ_{x_1}, real axis component of σ
σ_{11}, x_1-component of σ in the x_1-direction
σ_{12}, x_1-component of σ in the ix_2
σ_{22}, ix_2 component of σ in the ix_2
ε, ε_x, ε_{xx}, ε_y, ε_{yy}, ε_z, ε_{zz} strain and the components
L_1, original length and L_2 new length
u, v displacements
$\frac{du}{dx}$, displacement increments
E, elasticity modulus
F, force
S, stiffness
d, distance from crack-tip
v_{xy}, poisson ratio
τ shear stress
γ shear strain